Magnetite water based ferrofluid flow and convection heat transfer on a vertical flat plate: Mathematical and statistical modelling

Siti Hanani Mat Yasin, Muhammad Khairul Anuar Mohamed, Zulkhibri Ismail, Mohd Zuki Salleh [*]

Centre for Mathematical Sciences, Universiti Malaysia Pahang, 26300 UMP Kuantan, Pahang, Malaysia

A B S T R A C T

The unique magnetic properties of ferrofluid when exposed to the magnetic field led to the ferrofluid formulation in wide applications, especially as a thermal transfer. To picture the effective ferrofluid flow configurations and heat transfer mechanism at a surface, it is crucial to figure out the phenomenology of boundary layer and convective heat transfer. This study investigates a numerical solution of the mixed convection boundary layer flow of ferrofluid at the stagnation point on a vertical flat plate. Ferrofluid composed of magnetite (Fe_3O_4) water based exposure to the magnetic field and thermal radiation is considered. The complicated governing differential equations of fluid flow and heat transfer are simplified into simple equations using boundary layer approximation, Boussinesq approximation and similarity transformations. Then, the equations are solved numerically by employing the Keller-box method. Numerical results discovered that the ferroparticles volume fraction is the predominant factor in contributing to the trend of ferrofluid velocity, reduced skin friction and reduced Nusselt number. Further, the influence of the ferroparticles volume fraction on reduced skin friction and reduced Nusselt number are analyzed using regression analysis.

1. Introduction

Nanotechnology has given major efforts in developing an advanced fluid to help equipment become superior in terms of performance and providing a better cooling system. The revolution of miniaturization products highlights several attributes which need to be met but the conventional heat transfer fluids are incapable of providing good heat transfer performance and do not fulfil the system specifications. In most cases, the efficiency of nanofluid as a coolant agent occurs when increasing thermal conductivity [1]. Therefore, intensive research and development on the potential nanofluid were conducted to probe the fluid behaviour and the efficiency of heat transfer. One particular interest herein is the discovery of ferrofluid. Ferrofluid is composed of magnetic nanoparticles (maghemite (γ-Fe_2O_3), magnetite (Fe_3O_4), etc. with ~3-15 nm), liquid carrier (water, oil, ethylene glycol, etc.) and surfactants (lauric acid, oleic acid, etc.) [2–4]. The molecule of nanoparticles is coated with a surfactant agent to prevent agglomeration between nanoparticles. Ferrofluid is not found in nature but must be synthesized by chemical co-precipitation, decomposition of the iron carbonyl and so forth. Nevertheless, ferrofluid preparation at the nanoscale is quite challenging to stabilize because magnetic oxide exhibits

superparamagnetism magnetic behaviour and has high surface energy [2].

The applications of ferrofluid are extensively used in many areas such as electronic devices, military, aerospace, mechanical engineering, medicine, optics, heat transfer, analytical instrumentation and art [2,5,6]. The clinical research conducted by El-Boubbou [7] has explored the use of Fe_3O_4 for medical theranostic drug delivery in cancer therapeutics. The results show that Fe_3O_4 posed a potential cancer treatment, but this system has never been employed in human clinical settings although many formulations have been approved. Besides, ferrofluid as an advanced fluid for cooling technology in loudspeakers and electric motors employed to conduct heat away from the devices has been proven. Furthermore, ferrofluid in loudspeakers not only has benefits as a thermal transfer but it utilizes to reduce the power compression and damping resonances. Regarding the innovations and future expectations of the sound system industries, few formulations for mini or micro-speaker, in-ear devices, mobile platforms and forward-looking transducers and devices have yet to be imagined. This situation motivates authors to explore the behaviour of ferrofluid flow and heat transfer, which benefits the research and development of sound system technology industries or the other equipment that uses ferrofluid as a coolant fluid agent. Ferrofluid flow is found that deflected under a magnetic field and can minimize the temperature rise over the surface [4]. The black iron oxide (magnetite, Fe_3O_4) is found to be the most satisfactory in practice [8].

The potential of fluid as a coolant agent can be investigated by understanding the fluid flow properties and convection heat transfer on the surface [9]. The fundamental mechanism in determining heat transfer performance is the fluid properties over the surface area. From the viewpoint of industrial and engineering applications, the fluid flow and heat transfer on the surface such as in positioned vertical surfaces sparked a lot of studies. One of the applications is when the fins are placed vertically providing the best heat exchange along a surface compared to the horizontal surface [10]. The theoretical study has noticeably received the attention of scholars to predict the fluid characteristic on geometrical surfaces using boundary layer theory to avoid the cost of the experiment. The pioneer theoretical works by Ramachandran et al. [11] studied mixed convection heat transfer of viscous fluid towards stagnation flow on a vertical surface. Then, this problem extended using various fluid types such as micropolar fluid, Williamson fluid, Casson fluid, Jeffrey fluid and viscoelastic fluid [12–16]. Nonetheless, the fluid mentioned with large particles has some drawbacks regarding thermal conductivity, sedimentation and surface abrasion. Therefore, the studies of convection flow on the vertical plate in nanofluid and hybrid nanofluid have been carried out.

Recently, the boundary layer studies of ferrofluid flow and convection heat transfer on a vertical surface with Fe_3O_4 as a nanoparticle have been analyzed using diverse methods and technics. Khalid et al. [17] applied a Laplace transform technique to study the impact of thermal radiation effect upon magnetohydrodynamic (MHD) free convection Fe_3O_4-kerosene based flow passing through a porous medium. The results found the velocity decreases with the increasing value of the nanoparticles volume fraction parameter. Using the Keller-box method, Ilias et al. [18–20] numerically investigated the heat transfer rate of MHD free convection flow but using Fe_3O_4-water and kerosene based ferrofluid. These three studies obtained the same results when an increase in nanoparticles volume fraction and magnetic field strength elevates the Nusselt number although the fluid flow is steady or unsteady. Later, EL-Zahar et al. [21] solved numerically free convection Fe_3O_4-kerosene based ferrofluid flow using a new hybrid linearization-differential quadrature method (HLDQM). The results explained the ferrofluid flow generates a drag force when exposed to the magnetic field, which significantly changes its physical behaviour. The study of ferrofluid with Fe_3O_4 flow and heat transfer on a vertical plate is then extended and deliberated by the other researchers, as shown in Refs. [22–24], who only investigated the MHD mixed convection heat transfer.

Keeping in view the theoretical literature above [17,24], the impact of thermal radiation gives a progressively significant contribution to ferrofluid heat transfer. Solar energy is an example of thermal energy transfer by radiation with the capability to generate thermal and electrical energy. The efficiency of collecting and converting solar energy into something useful through solar thermal collectors such as the photovoltaic solar thermal collector (PV) and direct absorption solar collector (DASC) is very challenging. In terms of solar collector performance, the solar collector is not only effective in absorbing solar energy but have a good thermal transfer. According to Gu et al. [25–27], the utilization of nanofluid in the solar collector is more effective and efficient to transfer heat. The changing of nanoparticle properties such as particle size and particle volume fraction improve the performance of solar energy harvest [27].

Although the exploration in the analysis of ferrofluid flow and heat transfer on a vertical plate was particularly studied as mentioned above, no literature has been published concerning the statistical method for further analysis of the ferrofluid flow and heat transfer. Therefore, the present paper aims to study the MHD mixed convection flow of Fe_3O_4-water based ferrofluid with the existing the magnetic field and thermal radiation at stagnation flow on a vertical flat plate by implementing the mathematical and statistical method. In nanofluid studies, the nanoparticles volume fraction is one of the specific parameters that determine thermal conductivity which could be greatly influenced the characteristics of nanofluid [28–30]. The experiment results from Refs. [28–30] found an increase nanoparticles volume fraction in Fe_3O_4-water based led to an increase in the thermal conductivity at a certain temperature. The argument from the experiment results inspired the authors to investigate the correlation ferroparticles volume fraction to skin friction and Nusselt number. Hence, the governing equations in vector form are simplified to the Tiwari and Das model [31] to conduct this present study. Tiwari and Das model [31] known as the single-phase model stated that the liquid carrier and nanoparticles are in thermal equilibrium with the same velocity of flow and takes the volume fraction of nanoparticles into account to analyze the behaviour of nanofluid. This model assumed the nanoparticles have a uniform shape and size. Then, the equations are solved using a numerical approach by implementing the Keller-box method. The results from numerical data will be used in statistical analysis. It is noteworthy to mention that in this study the ferroparticles term is used to represent the nanoparticles in ferrofluid.

2. Governing equations of ferrofluid flow problem

The boundary layer flow of ferrofluid is two-dimensional, laminar, steady, incompressible and mixed convection heat transfer occurs at stagnation flow. The y-axis is normal to the x-axis along the direction of a stationary vertical surface with the presence of a magnetic field and thermal radiation as shown in Fig. 1. It is assumed that the free stream velocity is far from the body $U_\infty(x) = bx$ and the plate's temperature $T_w(x) = T_\infty + ax$ is proportional to the distance of x from the stagnation point where a and b are constants while T_∞ is the ambient temperature. Water (liquid carrier) and Fe_3O_4 (ferroparticles) are assumed to be single-phase fluids and have no-slip conditions with thermal equilibrium in ferrofluid. The ferroparticles are restricted to statistically homogeneous with uniformly sized and spherical particles as suggested by Brinkman [32] and Maxwell [33]. As the source term mentioned above, the movement of ferrofluid in a uniform magnetic field of strength B_o is applied at the positive y-direction perpendicular to the plate exerted to the Lorentz force in the momentum equation. The magnetic Reynolds number is assumed to be small; thus, the induced magnetic field and magnetic polarization are negligible. The fluid flow on the vertical plate in combined free and forced convection or called mixed convection has created the assisting and opposing flows [10]. Hence, the buoyancy force on the flow creates assisting flow (heated plate, $T_w > T_\infty$) and opposing flow (cooled plate, $T_w < T_\infty$) involved in the momentum equation. Furthermore, viscous dissipation and Joule heating are ignored while modelling the energy equation.

Under the assumptions above, the basic governing equations of the ferrofluid flow are formulated using the infinitesimally small fluid element with Eulerian differential formulation in the Cartesian coordinate. The continuity and momentum equations adopted the derivation as [34,35]:

The continuity equation:

$$\nabla \cdot \mathbf{V} = 0 \tag{1}$$

The momentum equation:

$$\rho_{ff}(\nabla \cdot \mathbf{V}) = \nabla p + \mu_{ff}\nabla^2 \mathbf{V} + (\mathbf{J} \times \mathbf{B}) + \rho_{ff}\mathbf{g} \tag{2}$$

where $\nabla = \left(\frac{\partial}{\partial x}, \frac{\partial}{\partial y}, \frac{\partial}{\partial z}\right)$ is vector operator, $\mathbf{V} = (u, v, w)$ is a velocity vector field, p is pressure, $\mathbf{J} = \sigma_{ff}(\mathbf{E} + \mathbf{V} \times \mathbf{B})$ is the current density (Lorentz force), $\mathbf{B} = (0, B_o, 0)$ is a total magnetic field, $\mathbf{E} = (0, 0, 0)$ is an electric field and $\mathbf{g} = (-g, 0, 0)$ is the gravitation acceleration $(\rho_{ff}\mathbf{g})$.

Next, the energy equation is derived using the first law of thermodynamics. Here, the effect of viscous dissipation, Joule heating and the rate of the energy equation are neglected. By considering the fundamental energy balance principle [35], this law can be written as

$$(\nabla \cdot \mathbf{V})T = \alpha_{ff}\nabla^2 T + \frac{1}{(\rho C_p)_{ff}}\nabla \mathbf{q_r}. \tag{3}$$

$\mathbf{q_r} = (-\nabla Q_r) \cdot (dx, dy, dz)$ is a net flux of thermal radiation where $Q_r = q_r A$ with q_r is the radiative heat flux and $A = (dydz, dxdz, dxdy)$ is surface area. The effective thermophysical properties expressions of ferrofluid (subscript ff) represents by σ is the electrical conductivity, ρ is the density, μ is the dynamic viscosity, α is the thermal diffusivity, T is the ferrofluid temperature and (ρC_p) is the effective heat capacity. It should be emphasized that the ferrofluid flow and heat transfer equations are derived in three-dimensional, and then reduce to two-dimensional. Eqs. (1)–(3) derived with respect to the boundary layer approximation by order of magnitude analysis and simplified using Boussinesq approximation yields

$$\frac{\partial u}{\partial x} + \frac{\partial v}{\partial y} = 0, \tag{4}$$
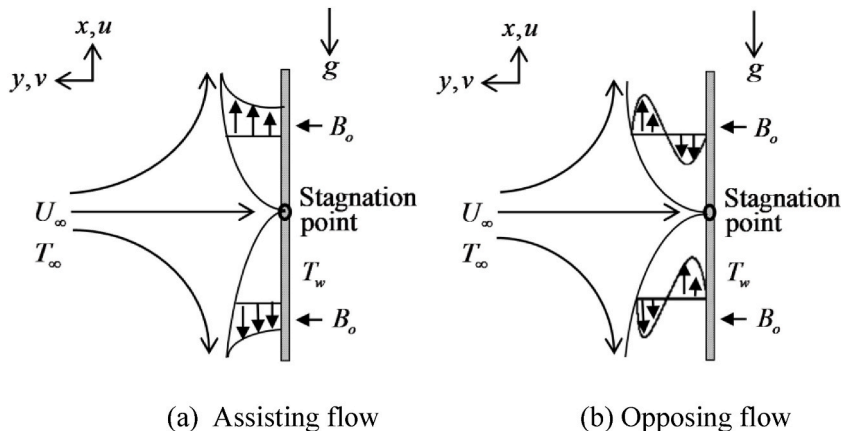

(a) Assisting flow   (b) Opposing flow

Fig. 1. Physical model and coordinate system.

$$u\frac{\partial u}{\partial x} + v\frac{\partial u}{\partial y} = U_\infty\frac{dU_\infty}{dx} + v_{ff}\frac{\partial^2 u}{\partial y^2} + \frac{(\rho\beta)_{ff}}{\rho_{ff}}g(T - T_\infty) - \frac{\sigma_{ff}B_o^2(x)}{\rho_{ff}}(u - U_\infty),$$
(5)

$$u\frac{\partial T}{\partial x} + v\frac{\partial T}{\partial y} = \alpha_{ff}\frac{\partial^2 T}{\partial y^2} - \frac{1}{(\rho C_p)_{ff}}\frac{\partial q_r}{\partial y}$$
(6)

subject to the boundary conditions [36] where the Blasius flow and constant wall temperature are considered as

$$u = v = 0, T = T_w \text{ at } y = 0,$$
$$u \rightarrow U_\infty, T \rightarrow T_\infty \text{ as } y \rightarrow \infty,$$
(7)

where u and v are the velocity components along the x and y-axes, respectively. Besides, v, β and k denotes the kinematic viscosity, thermal expansion and thermal conductivity. The subscript ff can be expressed in terms of liquid carrier, ferroparticles and ferroparticles volume fraction are adapted from Refs. [37–39] and the value of thermophysical properties considered as in Ref. [40]. The radiative heat flux term, q_r simplified using the Rosseland approximation [41,42] given by

$$q_r = -\frac{4\sigma^*}{3k^*}\frac{\partial T^4}{\partial y}$$
(8)

where σ^* and k^* denote the Stefan-Boltzmann constant and the mean absorption coefficient, respectively. The term T^4 expressed as a linear function of temperature expanding in a Taylor series about T_∞ implies that the temperature difference within the flow is sufficiently small and excludes the higher-order terms [43] in Eq. (6), then becomes

$$u\frac{\partial T}{\partial x} + v\frac{\partial T}{\partial y} = \alpha_{ff}\frac{\partial^2 T}{\partial y^2} + \frac{1}{(\rho C_p)_{ff}}\frac{16\sigma^*T_\infty^3}{3k^*}\frac{\partial^2 T}{\partial y^2}$$
(9)

The following similarity transformation is applied to obtain differential equations in dimensionless forms:

$$\eta = \left(\frac{b}{v_f}\right)^{1/2}y, \psi = (bv_f)^{1/2}xf(\eta), \theta(\eta) = \frac{T - T_\infty}{T_w - T_\infty}$$
(10)

where η is the non-dimensional similarity variable, θ is the fluid temperature and ψ is the stream function. Eq. (4) is satisfied and Eqs. (5) and (7) as well (9) were written as below by definition $u = \frac{\partial\psi}{\partial y}$ and $v = -\frac{\partial\psi}{\partial x}$.

$$\frac{1}{(1-\varphi)^{2.5}\left[1-\varphi+(\varphi\rho_s)/(\rho_f)\right]}f''' + ff'' - f'^2 + \frac{(1-\varphi)\rho_f + \varphi(\rho\beta)_s/\beta_f}{(1-\varphi)\rho_f + \varphi\rho_s}\lambda\theta$$
$$-\frac{\sigma_{ff}/\sigma_f}{(1-\varphi)+\varphi(\rho_s/\rho_f)}M(f'-1) = 0,$$
(11)

$$\frac{1}{\Pr}\left(\frac{(\rho C_p)_f}{(\rho C_p)_{ff}}\right)\left(\frac{k_{ff}}{k_f}+\frac{4}{3}Nr\right)\theta'' + f\theta' - f'\theta = 0$$
(12)

$$f(\eta) = 0, f'(\eta) = 0 = 0, \theta(\eta) = 1 \text{ at } \eta = 0$$
$$f'(\eta) \rightarrow 0, \theta(\eta) \rightarrow 0 \text{ as } \eta \rightarrow \infty$$
(13)

where f' and θ' represents the derivation with respect to the variable η with parameter involved as defined

$$M = \frac{\sigma_f B_o^2}{\rho_f b}, \Pr = \frac{v_f(\rho C_p)_f}{k_f}, Nr = \frac{4\sigma^*T_\infty^3}{k^*k_f}, \lambda = \frac{Gr_x}{\Re_x}$$
(14)

where λ is the mixed convection parameter, M is the magnetic parameter, Pr is the Prandtl number and Nr is the radiation parameter in which the local Grashof number and the local Reynolds number are expressed as

$$Gr = \frac{g\beta_f(T_w - T_\infty)x^3}{v_f^2}, \Re_x = \frac{U_\infty x}{v_f}$$
(15)

Here, it is noticed that λ is a constant with the flow impact of free convection corresponding to the buoyancy force effect in forced convection or the forced convection flow effect in free convection. Here, $\lambda < 0$ and $\lambda > 0$ denotes the opposing and assisting flows, respectively. The domination of forced convection is measured when $\lambda \rightarrow 0$ ($Gr_x = 0$) while $\lambda \rightarrow \infty$ ($\Re_x \approx 0$) describes the free convection [44]. At the hot surface, the buoyant motion is in the same direction as the forced motion but the direction is reversed to the forced motion at the cold surface. Next, the local skin friction coefficient C_f and the local Nusselt number Nu_x along the vertical wall are simplified into the dimensionless expression obtained as

$$C_f\mathrm{Re}_x^{1/2} = \frac{f''(0)}{(1-\varphi)^{2.5}}, Nu_x\mathrm{Re}_x^{-1/2} = -\left(\frac{k_{ff}}{k_f} + \frac{4}{3}Nr\right)\theta'(0) \tag{16}$$

3. Numerical and statistical analysis procedure

Eqs. (11) and (12) with boundary conditions (13) are solved numerically using the Keller-box method as derived by Yasin et al. [40, 45] and Cebeci and Bradshaw [46]. Next, the derivation of this method will be run in Matlab with step size, $\Delta\eta = 0.001$. Tables 1 and 2 show the present results indicating a good agreement with Groson and Pop's [47] results. Hence, the numerical computation suggests an accurate and acceptable result.

It is worth mentioning that when the value of the parameters equals zero, it means the parameter is absent from the equations such as $\varphi = 0$ which represents pure fluid water without the Fe_3O_4 particles. Besides, the value of the parameter in this study does not show the exact value like the experimental study because the purpose of this study is to show the estimating phenomenology trend when the pertinent parameter is increased or decreased. It is crucial to point out that all results found in this study do not exist in the dual solutions for assisting and opposing flows although the boundary layer thickness η_∞ has a large value. The fixed value (represents the parameter that exists in the ferrofluid flow) is taken at Pr = 6.2 (water), $\lambda = -2$ (opposing flow), $\lambda = 2$ (assisting flow), $M = 1$ and $Nr = 1$ to carry out the numerical computations. Meanwhile, the phenomenology trend of the ferroparticles volume fraction parameter is studied within the range of $0 \leq \varphi \leq 0.1$. The effects of ferroparticles volume fraction for assisting and opposing flow at a stagnation point on the vertical surface are discussed. Each parameter stated is chosen from the previous studies [19,22–24,48]. Based on the numerical data, a simultaneous regression analysis is proposed to predict the ferroparticles volume fraction that influences the $C_f\mathrm{Re}^{1/2}$ and $Nu_x\mathrm{Re}^{-1/2}$ using IBM SPSS software. Each pair of the observations satisfies the relationship of simple linear regression that can be expressed as

$$d_i = \widehat{\beta}_o + \widehat{\beta}_1 c_i + e_i \quad i = 1, 2, ..., n \tag{17}$$

where c_i is a predictor or independent variable, $\widehat{\beta}$ is a regression coefficient, d_i is a response or dependent variable and $e_i = d_i - \widehat{d}_i$ is a residual. In this study, d_i (actual observation) and $\widehat{d}_i$ (estimated) are the values of $C_f\mathrm{Re}^{1/2}$ and $Nu_x\mathrm{Re}^{-1/2}$. The residuals describe the error in the estimation of the model to the ith observation d_i. The estimated regression model which incorporates the ferroparticles volume fraction (φ) influences $C_f\mathrm{Re}^{1/2}$ and $Nu_x\mathrm{Re}^{-1/2}$ defined as

$$C_f\mathrm{Re}_{est}^{1/2} = \widehat{\beta}_o + \widehat{\beta}_1\varphi, Nu_x\mathrm{Re}_{est}^{-1/2} = \widehat{\beta}_o + \widehat{\beta}_1\varphi \tag{18}$$

Before further regression analysis was conducted, the data must be normally distributed and possess a linear relationship between the predictor and response variable. The boxplot test observed that the data are normally distributed and the linearity between variables is shown in the numerical results below. Then, the validity of the correlation coefficient is evaluated using probable error by applying the following formula

$$\mathrm{P.E}(r) = 0.6745 \frac{1 - r^2}{\sqrt{n}} \tag{19}$$

where r is the correlation coefficient and n is the number of observations.

4. Results and discussion

The effect of ferroparticles volume fraction φ on velocity profile $f'(\eta)$, temperature profile $\theta(\eta)$, reduced skin friction $C_f\mathrm{Re}^{1/2}$ and reduced Nusselt number $Nu_x\mathrm{Re}^{-1/2}$ are shown in Figs. 2–5. Correspondingly, Fig. 2 depicts the increment of parameter φ leading to a decrement $f'(\eta)$, which causes elevates the momentum boundary layer thickness for assisting flow. However, an opposite trend is observed in opposing flow. The circumstance trend of these two flows occurs due to the buoyancy force and Lorentz force direction. In assisting flow (heated plate, $T_w > T_\infty$), when the magnetic field is applied at the vertical plate as shown in Fig. 1, the direction of the Lorentz force becomes vertically downward direction. This is opposite to the ferrofluid flow and buoyancy force direction [49]. This phenomenon shows the Lorentz force tends to retards the fluid movement and decrease the ferrofluid velocity. Meanwhile, the reversed phenomenon occurs in the opposing flow (cooled plate, $T_w < T_\infty$). Even though the Lorentz force direction confronts the fluid

Table 1
Comparison of $C_f\mathrm{Re}^{1/2}$

λ	Groson and Pop [47]			Present		
	$\varphi = 0$	$\varphi = 0.1$	$\varphi = 0.2$	$\varphi = 0$	$\varphi = 0.1$	$\varphi = 0.2$
0	1.232587	1.884324	2.622743	1.232588	1.884324	2.622744
1	1.526774	2.172517	2.918305	1.526777	2.172518	2.918305
5	2.560232	3.223206	4.018088	2.560233	3.223206	4.018088
10	3.677522	4.392795	5.266077	3.677525	4.392800	5.266078
15	4.687465	5.464257	6.421169	4.687465	5.464258	6.421171

Table 2
Comparison of $Nu_x Re^{-1/2}$

λ	Groson and Pop [47]			Present		
	$\varphi = 0$	$\varphi = 0.1$	$\varphi = 0.2$	$\varphi = 0$	$\varphi = 0.1$	$\varphi = 0.2$
0	1.573432	1.969206	2.349363	1.573434	1.969207	2.349364
1	1.652418	2.033616	2.406390	1.652420	2.033617	2.406391
5	1.883998	2.240041	2.598275	1.884000	2.240043	2.598276
10	2.083819	2.432875	2.786792	2.083821	2.432877	2.786793
15	2.236582	2.586342	2.941284	2.236584	2.586343	2.941285
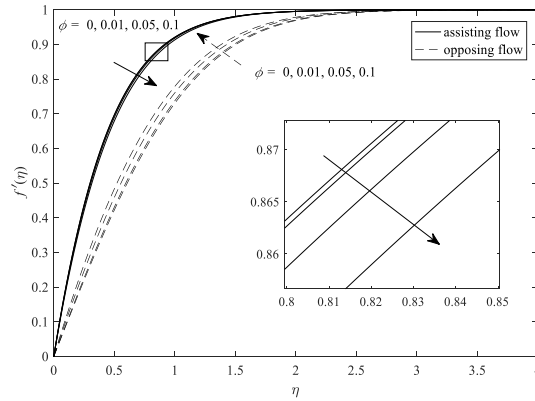
Fig. 2. Velocity profile $f'(\eta)$ for increasing of φ
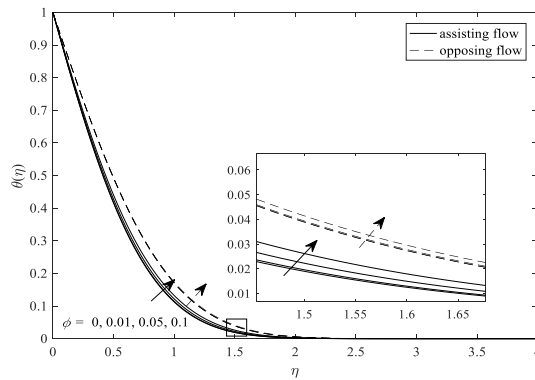
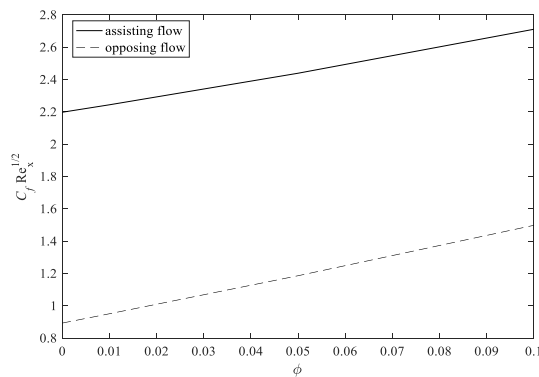**Fig. 3.** Temperature profile $\theta(\eta)$ for increasing of φ

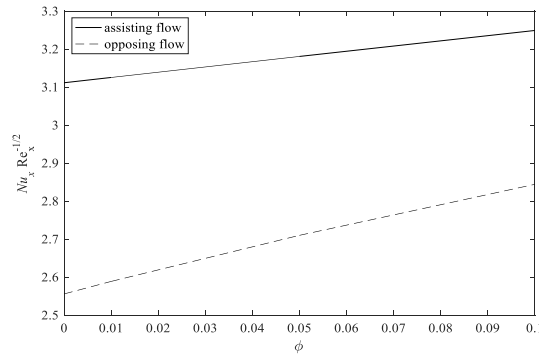**Fig. 4.** $C_f Re^{1/2}$ with several values of φ

6

Fig. 5. $Nu_x \mathrm{Re}^{-1/2}$ with several values of φ

movement direction, the velocity of opposing flow still increases due to the buoyancy force having the same direction as the Lorentz force direction that gravitates over the cooled plate [49]. Besides, it is perceived that one particular interest in influencing the velocity is the viscosity and temperature of ferrofluid. This argument is supported by experiment results conducted by Malekzadeh et al. [50], Toghraie et al. [51] and Sundar et al. [52] that observed the viscosity of Fe_3O_4-water based has increased with an upsurge in φ but diminished due to the increment of temperature. Fig. 3 shows the increase of φ elevates the parameter θ and thermal boundary layer thickness for both types of flow. Physically, the high temperature of the fluid will cause the intermolecular force of cohesion to decrease and random molecular motion to increase. Hence, this phenomenon makes the viscosity of the fluid decline and at the same time increases the velocity of the fluid but the different outcomes to the assisting flow velocity concern the buoyancy force and Lorentz force direction.

Figs. 4 and 5 illustrate the increment of φ are increase $C_f \mathrm{Re}^{1/2}$ and $Nu_x \mathrm{Re}^{-1/2}$ for both flows. The dimensionless Nusselt number is the measured component for determining the effectiveness of convective heat transfer flow through a fluid layer comprising eddies of recirculation. The results reduced Nusselt number in Fig. 5 observed proportional to the temperature of ferrofluid (see Fig. 4) when the ferroparticles volume fraction increased. This phenomenon demonstrates an enhanced rate of heat transport. Consequently, the magnetocaloric process is created in the ferrofluid flow in which the thermal energy is converted to the mechanical energy of motion [4]. This particular ideal process by Ref. [4] outlines fundamental principles for substantial improvement of the energy efficiency of a device. Apart from that, a considerable part of the Lorentz force goes into increasing the rate of heat transport and augmenting reduced skin friction coefficient.

The numerical results show that the ferroparticles volume fraction gives a significant linear relationship on the $C_f \mathrm{Re}^{1/2}$ and $Nu_x \mathrm{Re}^{-1/2}$. Further, Tables 3–6 shows the estimated value of $C_f \mathrm{Re}^{1/2}$ and $Nu_x \mathrm{Re}^{-1/2}$ for both flow with the various value of φ using the proposed regression model below:

The estimated $C_f \mathrm{Re}^{1/2}$ for assisting flow: $C_f \mathrm{Re}_{est}^{1/2} = 2.188 + 5.125\varphi$

The estimated $C_f \mathrm{Re}^{1/2}$ for opposing flow: $C_f \mathrm{Re}_{est}^{1/2} = 0.888 + 6.034\varphi$

The estimated $Nu_x \mathrm{Re}^{-1/2}$ for assisting flow: $Nu_x \mathrm{Re}_{est}^{-1/2} = 3.112 + 1.375\varphi$

The estimated $Nu_x \mathrm{Re}^{-1/2}$ for opposing flow: $Nu_x \mathrm{Re}_{est}^{-1/2} = 2.563 + 2.872\varphi$

The estimated value of $C_f \mathrm{Re}^{1/2}$ and $Nu_x \mathrm{Re}^{-1/2}$ in Tables 3–6 observed have the same increasing pattern when the ferroparticle volume fraction are enhanced with a small residual. The measurement of association between ferroparticles volume fraction and reduced skin friction as well as reduced Nusselt number are measured by the coefficient of determination (R^2). The linear association is closed to 100% of the variation in reduced skin friction and reduced Nusselt number explained by ferroparticles volume fraction shown in Table 7. Meanwhile, a strong linear relationship between two variables is generally certain when the value $r/\mathrm{P.E}(r)$ is greater than 6. As seen in Table 7, it demonstrates the coefficient of correlation is statistically significant and satisfies the linear relationship between ferroparticles volume fraction and reduced skin friction as well as reduced Nusselt number.

5. Conclusions

The magnetohydrodynamic (MHD) flow and heat transfer of Fe_3O_4-water based ferrofluid at the stagnation point on a vertical flat plate are scrutinized with the Blasius flow, thermal radiation and constant wall temperature are studied. The numerical analysis is implemented to investigate the significant impact of ferroparticles volume fraction on velocity, temperature, reduced skin friction and reduced Nusselt number. The findings of the study are as follows:

- The opposite phenomenon occurs due to the buoyancy force and Lorentz force for assisting and opposing flows on the velocity profile.
- An increasing ferroparticles volume fraction corresponding increases the reduced skin friction and reduced Nusselt number improve positively correlated between two variables.
- The significance of regression analysis proposed the equations model to forecast the effect of ferroparticles volume fraction.

Table 3
The estimated and actual value of $C_f\mathrm{Re}^{1/2}$ for assisting flow.

φ	$C_f\mathrm{Re}_{est}^{1/2}$	$C_f\mathrm{Re}^{1/2}$	e_i
0	2.18800	2.19756	0.00956
0.01	2.23925	2.24369	0.00444
0.05	2.44425	2.43891	−0.00534
0.1	2.70050	2.71087	0.01037

Table 4
The estimated and actual value of $C_f\mathrm{Re}^{1/2}$ for opposing flow.

φ	$C_f\mathrm{Re}_{est}^{1/2}$	$C_f\mathrm{Re}^{1/2}$	e_i
0	0.88800	0.89331	0.00531
0.01	0.94834	0.95087	0.00253
0.05	1.18970	1.18613	−0.00357
0.1	1.49140	1.49800	0.00660

Table 5
The estimated and actual value of $Nu_x\mathrm{Re}^{-1/2}$ for assisting flow.

φ	$Nu_x\mathrm{Re}_{est}^{-1/2}$	$Nu_x\mathrm{Re}^{-1/2}$	e_i
0	3.11200	3.11148	−0.00052
0.01	3.12575	3.12540	−0.00035
0.05	3.18075	3.18071	−0.00005
0.1	3.24950	3.24905	−0.00045

Table 6
The estimated and actual value of $Nu_x\mathrm{Re}^{-1/2}$ for opposing flow.

φ	$Nu_x\mathrm{Re}_{est}^{-1/2}$	$Nu_x\mathrm{Re}^{-1/2}$	e_i
0	2.56300	2.55581	−0.00720
0.01	2.59172	2.58876	−0.00297
0.05	2.70660	2.71002	0.00342
0.1	2.85020	2.84421	−0.00599

Table 7
Values of probable error.

$\varphi = 0$	Flow	R^2	P.E(r)	r/P.E(r)
$C_f\mathrm{Re}^{1/2}$	Assisting	0.99900	0.0000944	10587.73674
	Opposing	0.99999	0.0000009	1058773.674
$Nu_x\mathrm{Re}^{-1/2}$	Assisting	0.99999	0.0000009	1058773.674
	Opposing	0.99900	0.0000944	10577.14900

This phenomenon occurs provides critical insights into ferrofluid behaviour flow on a vertical flat plate that helps researchers to investigate the same problem in real application with the complex problem using the proposed regression model. Considering the limitation of Tiwari and Das model, the experiment study needs to further implement to investigate the magnetic properties and actual particle size of ferrofluid to ensure the stability and cooling performance on the verticle plate.

Declaration of competing interest

The authors declare that they have no known competing financial interests or personal relationships that could have appeared to influence the work reported in this paper.

Data availability

No data was used for the research described in the article.

Acknowledgement

References

[1] S.U.S. Choi, J.A. Eastman, Enhancing Thermal Conductivity of Fluids with Nanoparticles, ASME Int. Mech. Eng. Congr. Expo., San Francisco, USA, 1995, pp. 99–105.

[2] O. Oehlsen, S.I. Cervantes-Ramírez, P. Cervantes-Avilés, I.A. Medina-Velo, Approaches on ferrofluid synthesis and applications: current status and future perspectives, ACS Omega 7 (2022) 3134–3150.

[3] J.S. Mehta, R. Kumar, H. Kumar, H. Garg, Convective heat transfer enhancement using ferrofluid: a review, J. Therm. Sci. Eng. Appl. 10 (2018), 20801, https://doi.org/10.1115/1.4037200.

[4] R.E. Rosensweig, Ferrohydrodynamics, Cambridge University Press, New York, 1985.

[5] A.A. Siddiqui, M. Turkyilmazoglu, A new theoretical approach of wall transpiration in the cavity flow of the ferrofluids, Micromachines 10 (2019) 373.

[6] S. Tsuda, R.E. Rosensweig, Ferrofluid Centered Voice Coil Speaker, 2010.

[7] K. El-Boubbou, Magnetic iron oxide nanoparticles as drug carriers: clinical relevance, Nanomedicine 13 (2018) 953–971, https://doi.org/10.2217/nnm-2017-0336.

[8] S.S. Papell, Low Viscosity Magnetic Fluid Obtained by the Colloidal Suspension of Magnetic Particles, 1965.

[9] H. Schlichting, K. Gersten, Boundary-layer Theory, Ninth, Springer, Berlin, 2017.

[10] Y.A. Cengel, A.J. Ghajar, Heat and Mass Transfer: Fundamentals and Applications, sixth ed., McGraw-Hill Higher Education, 2020.

[11] N. Ramachandran, T.S. Chen, B.F. Armaly, Mixed convection in stagnation flows adjacent to vertical surfaces, J. Heat Tran. 110 (1988) 373–377, https://doi.org/10.1115/1.3250494.

[12] D. Mahanty, R. Babu, B. Mahanthesh, Theoretical and analytical analysis of convective heat transport of radiated micropolar fluid over a vertical plate under nonlinear Boussinesq approximation, Multidiscip. Model. Mater. Struct. 16 (2020) 915–936, https://doi.org/10.1108/MMMS-05-2019-0099.

[13] N. Nagendra, C.H. Amanulla, M.S. Reddy, V.R. Prasad, Hydromagnetic flow of heat and mass transfer in a nano Williamson fluid past a vertical plate with thermal and momentum slip effects: numerical study, Nonlinear Eng. 8 (2019) 127–144, https://doi.org/10.1515/nleng-2017-0057.

[14] A.S. Idowu, B.O. Falodun, Soret–Dufour effects on MHD heat and mass transfer of Walter'sB viscoelastic fluid over a semi-infinite vertical plate: spectral relaxation analysis, J. Taibah Univ. Sci. 13 (2019) 49–62.

[15] H. Kataria, H. Patel, Heat and mass transfer in magnetohydrodynamic (MHD) Casson fluid flow past over an oscillating vertical plate embedded in porous medium with ramped wall temperature, Propuls. Power Res 7 (2018) 257–267, https://doi.org/10.1016/j.jppr.2018.07.003.

[16] K. Ahmad, A. Ishak, Magnetohydrodynamic (MHD) Jeffrey fluid over a stretching vertical surface in a porous medium, Propuls. Power Res. 6 (2017) 269–276, https://doi.org/10.1016/j.jppr.2017.11.007.

[17] A. Khalid, I. Khan, S. Shafie, Heat transfer in ferrofluid with cylindrical shape nanoparticles past a vertical plate with ramped wall temperature embedded in a porous medium, J. Mol. Liq. 221 (2016) 1175–1183, https://doi.org/10.1016/j.molliq.2016.06.105.

[18] M.R. Ilias, N.A. Rawi, S. Shafie, Natural convection of ferrofluid from a fixed vertical plate with aligned magnetic field and convective boundary condition, Malaysian J. Fundam. Appl. Sci. 13 (2017) 223–228, https://doi.org/10.11113/mjfas.v13n3.651.

[19] M.R. Ilias, N.A. Rawi, N.H. Ab Raji, S. Shafie, Unsteady aligned MHD boundary layer flow and heat transfer of magnetic nanofluid past a vertical flat plate with leading edge accretion, ARPN J. Eng. Appl. Sci. 13 (2018) 340–351.

[20] M.R. Ilias, N.A. Rawi, S. Shafie, MHD free convection flow and heat transfer of ferrofluids over a vertical flat plate with aligned and transverse magnetic field, Indian J. Sci. Technol. 9 (2016) 1–7, https://doi.org/10.17485/ijst/2016/v9i36/97347.

[21] E.R. El-Zahar, A.M. Rashad, L.F. Seddek, The impact of sinusoidal surface temperature on the natural convective flow of a ferrofluid along a vertical plate, Mathematics 7 (2019) 1014, https://doi.org/10.3390/math7111014.

[22] A. Zaib, U. Khan, Z. Shah, P. Kumam, P. Thounthong, Optimization of entropy generation in flow of micropolar mixed convective magnetite (Fe3O4) ferroparticle over a vertical plate, Alex. Eng. J. 58 (2019) 1461–1470, https://doi.org/10.1016/j.aej.2019.11.019.

[23] A. Zaib, U. Khan, A. Wakif, M. Zaydan, Numerical Entropic Analysis of Mixed MHD convective flows from a non-isothermal vertical flat plate for radiative tangent hyperbolic blood biofluids conveying magnetite ferroparticles: dual similarity solutions, Arabian J. Sci. Eng. 45 (2020) 5311–5330, https://doi.org/10.1007/s13369-020-04393-x.

[24] A. Jamaludin, K. Naganthran, R. Nazar, I. Pop, Thermal radiation and MHD effects in the mixed convection flow of Fe3O4–water ferrofluid towards a nonlinearly moving surface, Processes 8 (2020) 95, https://doi.org/10.3390/pr8010095.

[25] M. Du, G.H. Tang, T.M. Wang, Exergy analysis of a hybrid PV/T system based on plasmonic nanofluids and silica aerogel glazing, Sol. Energy 183 (2019) 501–511.

[26] M. Du, G.H. Tang, Plasmonic nanofluids based on gold nanorods/nanoellipsoids/nanosheets for solar energy harvesting, Sol. Energy 137 (2016) 393–400.

[27] M. Du, G.H. Tang, Optical property of nanofluids with particle agglomeration, Sol. Energy 122 (2015) 864–872.

[28] Z. Liu, X. Wang, H. Gao, Y. Yan, Experimental study of viscosity and thermal conductivity of water based Fe3O4 nanofluid with highly disaggregated particles, Case Stud. Therm. Eng. 35 (2022), 102160.

[29] H. Haiza, I.I. Yaacob, A.Z.A. Azhar, Thermal conductivity of water based magnetite ferrofluids at different temperature for heat transfer applications, Solid State Phenom. 280 (2018) 36–42.

[30] M. Afrand, D. Toghraie, N. Sina, Experimental study on thermal conductivity of water-based Fe3O4 nanofluid: development of a new correlation and modeled by artificial neural network, Int. Commun. Heat Mass Tran. 75 (2016) 262–269.

[31] R.K. Tiwari, M.K. Das, Heat transfer augmentation in a two-sided lid-driven differentially heated square cavity utilizing nanofluids, Int. J. Heat Mass Tran. 50 (2007) 2002–2018, https://doi.org/10.1016/j.ijheatmasstransfer.2006.09.034.

[32] H.C. Brinkman, The viscosity of concentrated suspensions and solutions, J. Chem. Phys. 20 (1952) 571, https://doi.org/10.1063/1.1700493.

[33] J.C. Maxwell, A Treatise on Electricity and Magnetism, Clarendon Press, Oxford, 1873.

[34] M.R. Ilias, Steady and Unsteady Aligned Magnetohydrodynamics Free Convection Flows of Magnetic and Non Magnetic Nanofluids along a Wedge, Vertical and Inclined Plates, Universiti Teknologi Malaysia, 2018.

[35] J.F. Wendt, Computational Fluid Dynamics: an Introduction, third ed., Springer-Verlag Berlin Heidelberg, 2009.

[36] A. Nayan, N.I.F.A. Fauzan, M.R. Ilias, S.F. Zakaria, N.H.Z. Aznam, Aligned magnetohydrodynamics (MHD) flow of hybrid nanofluid over a vertical plate through porous medium, J. Adv. Res. Fluid Mech. Therm. Sci. 92 (2022) 51–64.

[37] A.A. Siddiqui, M. Turkyilmazoglu, Natural convection in the ferrofluid enclosed in a porous and permeable cavity, Int. Commun. Heat Mass Tran. 113 (2020), 104499.

[38] M. Sheikholeslami, A. Arabkoohsar, I. Khan, A. Shafee, Z. Li, Impact of Lorentz forces on Fe3O4-water ferrofluid entropy and exergy treatment within a permeable semi annulus, J. Clean. Prod. 221 (2019) 885–898, https://doi.org/10.1016/j.jclepro.2019.02.075.

[39] S. Hussain, S.E. Ahmed, Unsteady MHD forced convection over a backward facing step including a rotating cylinder utilizing Fe3O4-water ferrofluid, J. Magn. Magn Mater. 484 (2019) 356–366, https://doi.org/10.1016/j.jmmm.2019.04.040.

[40] S.H.M. Yasin, M.K.A. Mohamed, Z. Ismail, B. Widodo, M.Z. Salleh, Numerical investigation of ferrofluid flow at lower stagnation point over a solid sphere using, Keller-Box Method 94 (2022) 200–214, https://doi.org/10.37934/arfmts.94.2.200214.

[41] N.S. Wahid, N. Md Arifin, M. Turkyilmazoglu, M.E.H. Hafidzuddin, N.A. Abd Rahmin, MHD hybrid Cu-Al2O3/water nanofluid flow with thermal radiation and partial slip past a permeable stretching surface: analytical solution, in: J. Nano Res., Trans Tech Publ, 2020, pp. 75–91.

[42] N.S. Wahid, N.M. Arifin, M. Turkyilmazoglu, N.A.A. Rahmin, M.E.H. Hafidzuddin, Effect of magnetohydrodynamic Casson fluid flow and heat transfer past a stretching surface in porous medium with slip condition, in: J. Phys. Conf. Ser., IOP Publishing, 2019, 12028.

[43] V. Rajesh, M.A. Sheremet, H.F. Oztop, Impact of hybrid nanofluids on MHD flow and heat transfer near a vertical plate with ramped wall temperature, Case Stud. Therm. Eng. 28 (2021), 101557.

[44] I. Pop, D.B. Ingham, Convective Heat Transfer: Mathematical and Computational Modelling of Viscous Fluids and Porous Media, Elsevier, 2001.

[45] S.H.M. Yasin, M.K.A. Mohamed, Z. Ismail, M.Z. Salleh, Mathematical solution on MHD stagnation point flow of ferrofluid, Defect Diffusion Forum 399 (2020) 38–54. https://doi.org/10.4028/www.scientific.net/DDF.399.38.

[46] T. Cebeci, P. Bradshaw, Physical and Computational Aspects of Convective Heat Transfer, Springer-Verlag, New York, 1988.

[47] T. Grosan, I. Pop, Axisymmetric mixed convection boundary layer flow past a vertical cylinder in a nanofluid, Int. J. Heat Mass Tran. 54 (2011) 3139–3145, https://doi.org/10.1016/j.ijheatmasstransfer.2011.04.018.

[48] A. Bejan, Convection Heat Transfer, fourth, John Wiley & Sons, New York, 2013.

[49] R.J. Singh, T.B. Gohil, The numerical analysis on the development of Lorentz force and its directional effect on the suppression of buoyancy-driven flow and heat transfer using OpenFOAM, Comput. Fluids 179 (2019) 476–489, https://doi.org/10.1016/j.compfluid.2018.11.017.

[50] A. Malekzadeh, A.R. Pouranfard, N. Hatami, A.K. Banari, M.R. Rahimi, Experimental Investigations on the viscosity of magnetic nanofluids under the influence of temperature, volume fractions of nanoparticles and external magnetic field, J. Appl. Fluid Mech. 9 (2016) 693–697, https://doi.org/10.18869/ACADPUB.JAFM.68.225.24022.

[51] D. Toghraie, S.M. Alempour, M. Afrand, Experimental determination of viscosity of water based magnetite nanofluid for application in heating and cooling systems, J. Magn. Magn Mater. 417 (2016) 243–248, https://doi.org/10.1016/j.jmmm.2016.05.092.

[52] L.S. Sundar, M.K. Singh, A.C.M. Sousa, Investigation of thermal conductivity and viscosity of Fe3O4 nanofluid for heat transfer applications, Int. Commun. Heat Mass Tran. 44 (2013) 7–14, https://doi.org/10.1016/j.icheatmasstransfer.2013.02.014.